Anomaly detection in thermal pulse combustors using symbolic time series analysis

S Gupta[1], **A Ray**[1]*, and **A Mukhopadhyay**[2]
[1]Department of Mechanical Engineering, Pennsylvania State University, Pennsylvania, USA
[2]Department of Mechanical Engineering, Jadavpur University, Kolkata, India

The manuscript was received on 2 March 2006 and was accepted after revision for publication on 2 May 2006.

DOI: 10.1243/09596518JSCE256

Abstract: This paper presents symbolic time series analysis of observable process variables for anomaly detection in thermal pulse combustors. The anomaly detection method has been tested on the time series data of pressure oscillations, generated from a non-linear dynamic model of a generic thermal pulse combustor. Results are presented to exemplify early detection of combustion instability due to reduction of friction coefficient in the tailpipe, which eventually leads to flame extinction.

Keywords: anomaly detection, symbolic time series analysis, thermal pulse combustor

1 INTRODUCTION

Thermal pulse combustors are known to have a significantly higher thermal efficiency, higher heat transfer rate, and lower pollutant emission than steady flow combustors. As a result of strong coupling between thermofluid dynamics in the combustor and the tailpipe, pulse combustors are often subjected to self-sustained pressure oscillations [**1**]. Knowledge of the non-linear dynamics of the underlying process is essential for prediction of potential instabilities in combustors [**2**]. From this perspective, the non-linear dynamics of pulse combustors have been investigated both analytically and experimentally by several researchers [**3**, **4**].

Gradual occurrence of parametric and non-parametric changes in the combustion process may cause unpredictable anomalies (i.e. deviations from the nominal behaviour) and thereby lead to significant degradation in the combustor performance over time [**5**]. The resulting evolution of anomalies is often very difficult to detect from measurements of the process variables unless the embedded statistical information is extracted via analytical tools of signal processing and pattern identification [**6**, **7**]. Time series analysis of measured variables (e.g. combustor pressure) can be used for identification of behaviour patterns in pulse combustors owing to the gradual reduction in the friction coefficient in the tailpipe. The rationale for selecting the tailpipe friction coefficient as a parameter for anomaly detection [**4**, **8**] is summarized as follows.

1. The combustor performance is strongly influenced by the tailpipe drag force which is expressed in terms of the friction coefficient in the present low-dimensional model [**1**]. Variations in the drag force may result from gradual changes in combustor flow conditions as well as from wear and corrosion upon prolonged operation.
2. Small changes in the friction coefficient are difficult to detect at early stages but can be estimated by observing the effects of its changes on the system response (e.g. pressure oscillations).
3. Early detection of changes in the tailpipe friction coefficient potentially facilitates synthesis of real-time control strategies for life-extending control and damage mitigation [**5**, **9**, **10**].
4. Changes in other parameters (e.g. wall temperature) produce transitions of combustion characteristics that are similar to that observed owing to changes in the friction coefficient [**11**]. Hence, the conclusions of this investigation can be generalized and extended to other anomalies also.

A novel information-theoretical technique of pattern identification is applied for early detection of anomalies resulting from reduction in the tailpipe

* *Corresponding author: Department of Mechanical Engineering, Pennsylvania State University, 329 Reber Building, University Park, PA 16802, USA. email: axr2@psu.edu*

friction coefficient. The time series data of combustor pressure oscillations are processed and subsequently converted from the domain of real numbers into the domain of (discrete) symbols. The resulting symbol sequence is a transform of the original time series sequence such that the loss of information is minimized in the sense of maximized entropy. Then, tools of computational mechanics [**12**, **13**] are used to find patterns in the symbolic sequences through construction of a finite state machine [**13**].

Symbolic time series analysis (STSA) for anomaly detection is an information-theoretical pattern identification tool that is built upon a fixed-structure Markov chain, called the *D*-Markov machine [**13**]. Recent literature [**14**, **15**] has reported experimental validation of STSA-based pattern identification by comparison with other existing techniques such as principal component analysis (PCA) and artificial neural networks (ANNs); STSA has been shown to yield superior performance in terms of early detection of anomalies, robustness to noise, and real-time execution in different applications such as electronic circuits, electric motors, and fatigue damage in polycrystalline alloys.

The paper is organized in five sections including the present section. Section 2 describes the simulation model of the combustion process in a generic thermal pulse combustor [**1**]. Section 3 describes the underlying concepts and essential features of STSA for anomaly detection [**13**]. Section 4 presents the results of STSA-based anomaly detection. The paper is summarized and concluded in section 5.

2 DESCRIPTION OF COMBUSTOR MODELLING

This section presents a non-linear dynamic model of a generic thermal pulse combustor, originally formulated by Richards *et al.* [**1**]. Figure 1 shows a schematic diagram of the combustor consisting of the combustion zone and the tailpipe. The combustor model largely characterizes self-sustained pressure oscillations that accrue from the strong coupling between combustion dynamics and gas flow in the tailpipe. The mechanism driving these oscillations is briefly described below.

Following the initial transients, both the pressure and the temperature start to increase within the combustor, accompanied by a decrease in the fuel mass fraction. The increased pressure leads to an enhanced rate of mass efflux into the tailpipe. As the outflow rate exceeds the inflow rate, the combustor pressure starts to drop. Similarly, increased gas temperature enhances the reaction rate, causing a reduction in the fuel mass fraction. This phenomenon reduces the reaction rate, with consequent decreases in gas temperature and pressure. As the combustor pressure falls below the tailpipe pressure, flow reversal takes place. Meanwhile, the fuel concentration builds up owing to continuous inflow of the reacting mixture and reduced rate of fuel consumption due to lower temperature. The fuel build-up resumes a vigorous chemical reaction, leading to repetition of the above cycle.

The drag force is represented in the present model by the tailpipe friction coefficient [**10**]. The friction coefficient has also been used as a parameter for controlling chaos [**5**]. In this paper, the tailpipe friction coefficient is assumed to decrease owing to wear, fatigue, and corrosion in the mechanical structure of the tailpipe (see section 1); consequently, the flow conditions are altered. The details of the friction coefficient computation are not presented in this paper.

Since the focus of the paper is to demonstrate an application of STSA to detect small changes in the critical system parameter(s) in thermal pulse combustors, a low-dimensional model that has been shown to capture the essential dynamics of the system [**1**, **5**, **10**] has been adopted.

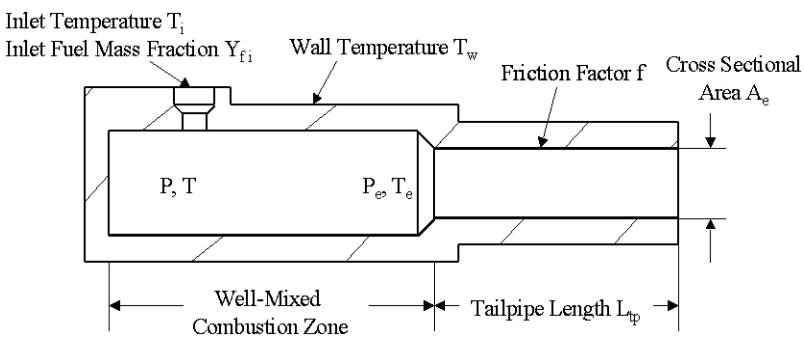

Fig. 1 Schematic diagram of a generic thermal pulse combustor with specified inlet and tailpipe parameters

The major assumptions in the development of the pulse combustor model are as follows:

(a) perfect mixing and macroscopic homogeneity in the combustor;
(b) constant specific heat and ideal gas properties for the reactants and the products of combustion;
(c) slug flow in the tailpipe;
(d) single-step Arrhenius model for chemical kinetics;
(e) convective heat transfer from gas to the combustor wall.

With these assumptions, the non-linear dynamic model is described in terms of four first-order coupled differential equations, resulting in four dimensionless state variables: temperature $\tilde{T}$, pressure $\tilde{P}$, fuel mass fraction Y_f, and exit velocity $\tilde{u}$. While a detailed derivation of the model equations has been reported in reference [**1**], the governing equations are summarized below.

Lumped representation of conservation of energy in the reactor yields

$$\frac{d\tilde{T}}{dt} = \frac{\gamma\tilde{T}}{\tilde{P}}\left(\frac{1}{\tau_f} + \frac{1}{\tau_h} + \frac{1}{\tau_c}\right) - \frac{\tilde{T}^2}{\tilde{P}}\left[\frac{1}{\tau_f} + \frac{(\gamma-1)Z_e}{\rho_0} + \frac{\gamma}{\tilde{T}_w\tau_h}\right] \quad (1)$$

The characteristic time parameters, flow time τ_f, heat transfer time τ_h, and chemical reaction time τ_c, are defined as

$$\tau_f = \frac{\rho_0}{Z_i}, \qquad \tau_h = \frac{L_{c1}\rho_0 C_p}{h\tilde{T}_w}, \qquad \tau_c = \frac{\rho_0 C_p T_0}{\dot{R}_f \Delta h_c} \quad (2)$$

Combining equation (1) with conservation of mass yields the pressure dynamics as

$$\frac{d\tilde{P}}{dt} = \gamma\left(\frac{1}{\tau_f} + \frac{1}{\tau_h} + \frac{1}{\tau_c}\right) - \gamma\tilde{T}\left(\frac{Z_e}{\rho_0} + \frac{1}{\tilde{T}_w\tau_h}\right) \quad (3)$$

Conservation of fuel mass yields the dynamics of fuel mass fraction as

$$\frac{dY_f}{dt} = \frac{\tilde{T}}{\tilde{P}}\frac{1}{\tau_f}(Y_{fi} - Y_f) - \frac{C_p T_0}{\Delta h_c}\frac{\tilde{T}}{\tilde{P}}\left(\frac{1}{\tau_c}\right) \quad (4)$$

Finally, momentum balance yields the gas velocity dynamics in the tailpipe as

$$\frac{d\tilde{u}}{dt} = \frac{RT_0\tau_f}{L_{c2}L_{tp}}\frac{\tilde{T}_e}{\tilde{P}_e}(\tilde{P}_e - 1) - \frac{f|\tilde{u}|\tilde{u}L_{c2}}{2D_{tp}\tau_f} \quad (5)$$

The combustion time τ_c is calculated on the basis of single-step global Arrhenius kinetics for stoichiometric mixtures at the inlet such that

$$\dot{R}_f = -B\nu_0 T^{1/2}\rho^2 Y_f^2 \exp\left(-\frac{T_a}{T}\right) \quad (6)$$

where B is a kinetic constant, T_a is the activation temperature, and ν_0 is the stoichiometric oxygen–fuel ratio by mass [**1**]. As such, equations (2) and (6) yield the chemical reaction time

$$\tau_c = \left[\frac{B'\Delta h_c}{C_p T_0}\frac{\tilde{P}^2}{\tilde{T}^{3/2}}Y_f^2 \exp\left(-\frac{\tilde{T}_a}{\tilde{T}}\right)\right]^{-1} \quad (7)$$

where the constant terms are merged into B'. An expression for Z_e, which is needed to close the system of equations, is obtained from conservation of mass within the tailpipe as

$$Z_e = \rho_0\frac{\tilde{u}}{\tau_f}\frac{\tilde{P}_e}{\tilde{T}_e} \quad (8)$$

Finally, flow in the nozzle connecting the combustor and the tailpipe is assumed to be isentropic, owing to the short length of this section, although irreversibilities are present in both the combustor and the tailpipe. Thus, the pressure and temperature in the tailpipe are related to the combustor variables through isentropic relations as

$$\tilde{T}_e = \tilde{T} - \frac{\tilde{u}^2 L_{c2}^2}{2C_p T_0 \tau_f^2}, \quad \tilde{P}_e = \tilde{P}\left(\frac{\tilde{T}_e}{\tilde{T}}\right)^{\gamma/(\gamma-1)} \quad (9)$$

The pulse combustor model follows the type and geometry reported in reference [**1**]; the kinetic parameters are listed in Table 1. Propane is used as the fuel stoichiometrically mixed with air. To initiate the reaction, the initial temperature is raised to five times the ambient temperature. The choice of the initial time step affects only the initial transients that last for a period $t \leqslant 0.2$ s. The anomaly detection analysis, presented in this paper, is based on time series data in the range of $1.0\ \text{s} \leqslant t \leqslant 1.2$ s. The dynamic characteristics of all the state variables, i.e. temperature, pressure, fuel mass fraction, and exit velocity, are similar. However, for data acquisition in the experimental environment, the measurement devices (i.e. sensors and ancillary equipments) must be tolerant of high temperatures and have very small response times. Therefore, temperature and fuel mass fraction measurements are not considered for

Table 1 Model parameters

Parameter	Value	Parameter	Value
A_s	0.0167 m^2	h	120 W/m^2 K
V	1.985×10^{-4} m^3	P_0	1×10^5 Pa
B'	3.85×10^8	T_a	50 K
C_p	1200 J/kg K	T_0	300 K
D_{tp}	0.0178 m	T_w	1000 K
L_{c1}	0.0119 m	γ	1.27
L_{c2}	0.7434 m	ρ_0	1.12 kg/m^3
L_{tp}	0.61 m	t_f	0.027 s
Y_{fi}	0.06	Δh_c	4.6×10^7 J/kg

analysis as the corresponding sensors may not survive in the harsh environment of the combustion chamber and/or may suffer from relatively slow response. Hence, the time series data of combustor pressure have been used in this paper for anomaly detection.

The governing equations are solved as a system of coupled non-linear ordinary differential equations using the library function ODE45 of the commercial package MATLAB. This function uses a fourth-order variable-step Runge–Kutta method. The data sampling rate is about 0.1 MHz. Thus, the generated data set is sufficiently large for post-processing analysis.

3 SYMBOLIC TIME SERIES ANALYSIS

This section presents the underlying concepts and essential features of STSA [**16**] for anomaly detection in complex dynamic systems. While the details have been reported in previous publications [**13**, **17**], the key features of STSA are succinctly described below for clarity and completeness.

The sampling frequency for data acquisition is required to be at least twice the highest frequency of the process response, while the evolution of anomalies (e.g. reduction in the tailpipe friction coefficient) occurs gradually over a much longer time period compared with the process response time. Therefore, the anomaly monitoring and detection process is formulated as a two-time scale problem.

1. The *fast timescale* is related to the response time of thermo-acoustics (i.e. pressure oscillations). Over the span of a given time series data sequence, the combustion dynamics essentially remain invariant, i.e. the process is assumed to exhibit stationary dynamics on the fast timescale. In other words, the variations in the statistical behavior of combustion dynamics are negligible on the fast timescale.
2. The *slow timescale* is related to the time span over which the process may exhibit non-stationary behaviour (e.g. owing to gradual evolution of wear, fatigue, and corrosion in the mechanical structures). In other words, an observable non-stationary behaviour can be associated with anomalies evolving on the slow timescale. In general, a long time span on the fast timescale is a tiny (i.e. many orders of magnitude smaller) interval on the slow timescale. For example, evolution of reduction in the tailpipe friction coefficient, causing a detectable change in the combustion dynamics, takes place on the slow timescale (possibly of the order of months) and is essentially invariant on the fast time scale (approximately of the order of seconds or minutes).

Nevertheless, the notion of fast and slow timescales is dependent on the specific application, exogenous excitation, and operating environment. As such, from the perspective of combustion stability monitoring, sensor data acquisition is carried out on the fast timescale at different slow time epochs. Further details are presented in section 4.

3.1 Transformation from continuous to symbolic domain

A time series data sequence is converted to a symbol sequence by partitioning a compact region Ω of the phase space, over which the trajectory evolves, into finitely many discrete blocks as seen in Fig. 2. Let $\{\Phi_1, \Phi_2, \ldots, \Phi_m\}$ be a partitioning of Ω, such that it is exhaustive and mutually exclusive, and thus

$$\bigcup_{j=1}^{m} \Phi_j = \Omega, \quad \Phi_j \bigcap \Phi_k = \varnothing \; \forall j \neq k \tag{10}$$

Each block Φ_j is labelled as a symbol $\sigma_j \in \Sigma$, where the symbol set Σ is called the *alphabet* consisting of m different symbols (i.e. $m = |\Sigma|$). As the system evolves in time, the trajectory travels through various blocks in its phase space and the corresponding symbol $\sigma_j \in \Sigma$ is assigned to it, thus converting the time series data sequence to a symbol sequence $\cdots \sigma_{i_i} \sigma_{i_2} \cdots \sigma_{i_k} \cdots$. Thus, the symbol sequences represent coarse graining of the trajectories' time evolution [**18**]. Once the symbol sequence is obtained, the next step is the construction of the finite state machine (see section 3.3) and calculation of the state visit frequencies to generate the state probability vector as depicted in Fig. 2 by the histograms. The comparison of these state probability vectors at different time epochs from the nominal condition determines the changes in the patterns of system dynamics on the slow timescale.

3.2 Wavelet-based partitioning for symbol generation

A crucial step in STSA is partitioning of the phase space for symbol sequence generation [**16**]. Several partitioning techniques have been reported in literature for symbol generation [**6**, **19**, **20**], primarily based on symbolic false neighbours. These techniques rely on partitioning the phase space and may become cumbersome and extremely computation

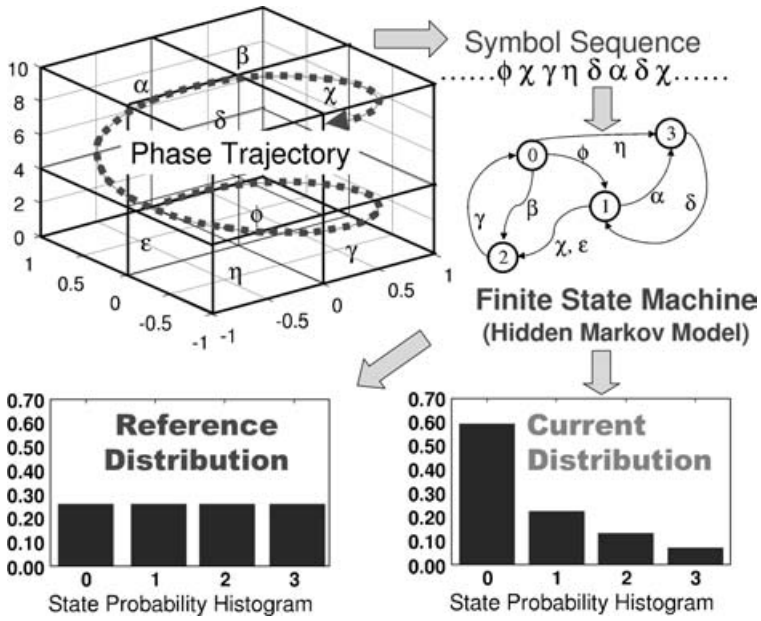

Fig. 2 Example of space partitioning

intensive if the dimension of the phase space is large. Moreover, if the time series data are noise corrupted, then the symbolic false neighbours would rapidly grow in number and require a large symbol alphabet to capture the pertinent information on the system dynamics. Therefore, symbolic sequences as representations of the system dynamics should be generated by alternative methods because phase-space partitioning might prove to be a difficult task for systems of high dimensions and in the presence of noise. The wavelet transform [**21**] largely alleviates these shortcomings and is particularly effective with noisy data from high-dimensional dynamic systems [**17**, **22**].

This paper has adopted a wavelet-based partitioning approach [**13**] for construction of symbol sequences from time series data. In this method, the time series data are first converted to the wavelet domain, where wavelet coefficients are generated on different scales and at various time shifts. These coefficients are stacked at selected time-shift positions, starting with the smallest value of the scale and ending with its largest value and then back from the largest value to the smallest value of the scale at the next instant of time shift.

The above one-dimensional array of rearranged wavelet coefficients is termed as the *scale series data*, which are structurally similar to time series data. The data sequence is partitioned into $|\Sigma|$ segments of wavelet coefficients on the ordinate separated by horizontal lines, as seen in Fig. 3. The partitioning is carried out such that the regions with more information are partitioned finely and those with

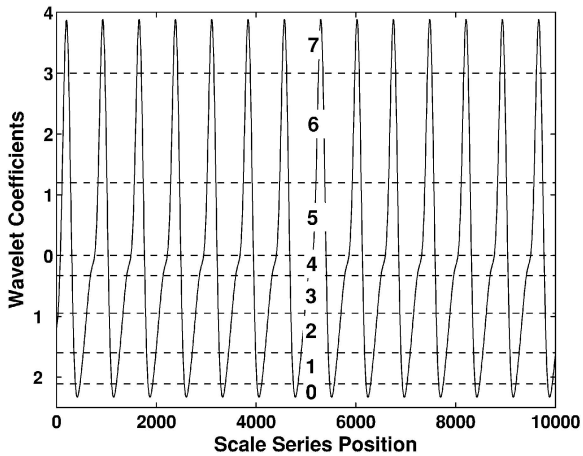

Fig. 3 Wavelet-space maximum-entropy partitioning

sparse information are partitioned coarsely. This is achieved by maximizing the Shannon entropy [**23**], which is defined as

$$S = -\sum_{i=1}^{|\Sigma|} p_i \log(p_i) \tag{11}$$

where p_i is the probability of the ith state and the summation is taken over all possible states. The uniform probability distribution of states is a consequence of maximum entropy that makes the partition coarser in regions of low data density and finer in regions of high data density. Figure 3 shows an example of the maximum-entropy partitioning in the wavelet space for alphabet size $|\Sigma| = 8$, where the partition segments are indicated by symbols ranging from 0 to 7.

Once the partitioning has been made with alphabet size $|\Sigma|$ at the nominal condition (time epoch t_0), it is kept constant for all (slow time) epochs $\{t_1, t_2, \ldots, t_k, \ldots\}$, i.e. the structure of the partition is fixed at the nominal condition. In other words, the partitioning structure generated at the nominal condition serves as the reference frame for data analysis at subsequent slow time epochs.

3.3 State machine construction

The partitioning as described in the previous section is performed at the slow time epoch t_0 of the nominal condition, which is chosen to be the healthy state having zero anomaly measure. A finite state machine is then constructed, where the states of the machine are defined corresponding to a given *alphabet set* Σ and window length D. The alphabet size $|\Sigma|$ is the total number of partition segments while the window length D is the length of consecutive symbol words [**13**], which are chosen as all possible words of length D from the symbol sequence. Each state belongs to an equivalence class of symbol words of length D or more, which is characterized by a word of length D at the leading edge. Therefore, the number n of such equivalence classes (i.e. states) is less than or equal to the total permutations of the alphabet symbols within words of length D, i.e. $n \leqslant |\Sigma|^D$; some of the states may be forbidden with zero probability of occurrence. For example, if $\Sigma = \{0, 1\}$, i.e. $|\Sigma| = 2$, and if $D = 2$, then the number of states is $n \leqslant |\Sigma|^D = 4$, and the possible states are 00, 01, 10, and 11, as shown in Fig. 4.

The choice of $|\Sigma|$ and D depends on specific experiments, noise level, and also the available computation power. A large alphabet may be noise sensitive while a small alphabet could miss the details of signal dynamics [**17**]. Similarly, while a larger value of D is more sensitive to signal distortion, it would create a much larger number of states, requiring more computation power. In this paper, the parameters are chosen as $D = 1$ and $|\Sigma| = 8$, leading to a finite state machine with eight states, which is very fast in computation and is also capable of early detection of anomalies (e.g. changes in the tailpipe friction coefficient). Using the symbol sequence generated from the time series data, the state machine is constructed on the principle of sliding block codes [**24**], as explained below.

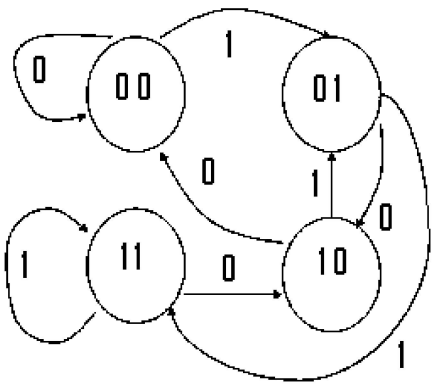

Fig. 4 Finite state automaton with $D = 2$ and $\Sigma = \{0, 1\}$

The window of length D in the symbol sequence $\cdots \sigma_{i_1} \sigma_{i_2} \cdots \sigma_{i_k} \cdots$ is shifted to the right by one symbol, such that it retains the last $D - 1$ symbols of the previous state and appends it with the new symbol σ_{i_l} at the end. The symbolic permutation in the current window gives rise to a new state. The machine constructed in this fashion is called the D-Markov machine [**13**], because of its Markov properties.

Definition 1

A symbolic stationary process is called D-Markov if the probability of the next symbol depends only on the previous D symbols, i.e.

$$P(\sigma_{i_0}|\sigma_{i_{-1}} \cdots \sigma_{i_{-D}}\sigma_{i_{-D-1}} \cdots) = P(\sigma_{i_0}|\sigma_{i_{-1}} \cdots \sigma_{i_{-D}})$$

The finite state machine constructed above has D-Markov properties because the probability of occurrence of symbol σ_{i_l} on a particular state depends only on the configuration of that state, i.e. the previous D symbols. Once the alphabet size $|\Sigma|$ and word length D are determined at the nominal condition (i.e. time epoch t_0), they are kept constant for all slow time epochs $\{t_1, t_2, \ldots, t_k, \ldots\}$ (see section 3.2). That is, the partitioning and the state machine structure generated at the nominal condition serve as the reference frame for data analysis at subsequent slow time epochs.

The states of the machine are marked by the corresponding symbolic word permutation and the edges joining the states indicate the occurrence of a symbol σ_{i_l}. The occurrence of a symbol at a state may keep the machine in the same state or move it to a new state. For $D = 1$, the set of states bears a bijective relation to the alphabet Σ of symbols.

Definition 2

The probability of transitions from state q_j to state q_k belonging to the set Q of states under a transition $\delta : Q \times \Sigma \to Q$ is defined as

$$\pi_{jk} = P(\sigma \in \Sigma | \delta(q_j, \sigma) \to q_k), \qquad \sum_k \pi_{jk} = 1 \tag{12}$$

Thus, for a D-Markov machine, the irreducible stochastic matrix [**25**] $\mathbf{\Pi} \equiv [\pi_{ij}]$ describes all transition

probabilities between states such that it has at most $|\Sigma|^{D+1}$ non-zero entries. The left eigenvector $\boldsymbol{p}$ corresponding to the unit eigenvalue of $\boldsymbol{\Pi}$ is the state probability vector under the (fast time scale) stationary condition of the dynamic system [**13**]. On a given symbol sequence $\cdots \sigma_{i_1} \sigma_{i_2} \cdots \sigma_{i_l} \cdots$ generated from the time series data collected at a slow time epoch, a window of length D is moved by keeping a count of occurrences of word sequences $\sigma_{i_1} \cdots \sigma_{i_D} \sigma_{i_{D+1}}$ and $\sigma_{i_1} \cdots \sigma_{i_D}$, which are denoted by $N(\sigma_{i_1} \cdots \sigma_{i_D} \sigma_{i_{D+1}})$ and $N(\sigma_{i_1} \cdots \sigma_{i_D})$ respectively. Note that, if $N(\sigma_{i_1} \cdots \sigma_{i_D}) = 0$, then the state $q \equiv \sigma_{i_1} \cdots \sigma_{i_D} \in Q$ has zero probability of occurrence. For $N(\sigma_{i_1} \cdots \sigma_{i_D}) \neq 0$, the transitions probabilities are then obtained by these frequency counts as

$$\pi_{jk} \equiv P(q_k|q_j) = \frac{P(q_k, q_j)}{P(q_j)} = \frac{P(\sigma_{i_1} \cdots \sigma_{i_D}\sigma)}{P(\sigma_{i_1} \cdots \sigma_{i_D})}$$

$$\Rightarrow \pi_{jk} \approx \frac{N(\sigma_{i_1} \cdots \sigma_{i_D}\sigma)}{N(\sigma_{i_1} \cdots \sigma_{i_D})} \tag{13}$$

where the corresponding states are denoted by $q_j \equiv \sigma_{i_1} \sigma_{i_2} \cdots \sigma_{i_D}$ and $q_k \equiv \sigma_{i_2} \cdots \sigma_{i_D} \sigma$. The time series data under the nominal condition (set as a benchmark) generates the *state transition matrix* $\boldsymbol{\Pi}^0$ which, in turn, is used to obtain the *state probability vector* $\boldsymbol{p}^0$ whose elements are the stationary probabilities of the state vector, where $\boldsymbol{p}^0$ is the left eigenvector of $\boldsymbol{\Pi}^0$ corresponding to the (unique) unit eigenvalue. Subsequently, state probability vectors $\boldsymbol{p}^1, \boldsymbol{p}^2, \ldots, \boldsymbol{p}^k, \ldots$ are obtained at slow time epochs $t_1, t_2, \ldots, t_k, \ldots$ based on the respective time series data. As stated earlier, the machine structure and partitioning are the same at all slow time epochs.

3.4 Stopping rule for determining symbol sequence length

This section presents a stopping rule that is necessary to find a lower bound on the length of symbol sequence required for parameter identification of the stochastic matrix $\boldsymbol{\Pi}$. The stopping rule [**26**] is based on the properties of irreducible stochastic matrices [**25**]. The state transition matrix is constructed at the rth iteration (i.e. from a symbol sequence of length r) as $\boldsymbol{\Pi}(r)$ that is an $n \times n$ irreducible stochastic matrix under stationary conditions. The state probability vector $\boldsymbol{p}(r) \equiv [\, p_1(r) \quad p_2(r) \quad \cdots \quad p_n(r)]$ is obtained as

$$p_i(r) = \frac{r_i}{\sum_{j=1}^{n} r_i} \tag{14}$$

where r_i is the number of symbols in the ith state such that $\sum_{i=1}^{n} r_i = r$ for a symbol sequence of length r. The stopping rule makes use of the Perron–Frobenius theorem [**25**] to establish a relation between the vector $\boldsymbol{p}(r)$ and the matrix $\boldsymbol{\Pi}(r)$. Since the matrix $\boldsymbol{\Pi}(r)$ is stochastic and irreducible, there exists a unique eigenvalue $\lambda = 1$ and the corresponding left eigenvector $\boldsymbol{p}(r)$ (normalized to unity in the sense of absolute sum). The left eigenvector $\boldsymbol{p}(r)$ represents the state probability vector, provided that the matrix parameters have converged after a sufficiently large number of iterations. That is

$$\boldsymbol{p}(r) = \boldsymbol{p}(r)\boldsymbol{\Pi}(r) \quad \text{as } r \to \infty \tag{15}$$

Following equation (14), the absolute error between successive iterations is obtained such that

$$\|(\boldsymbol{p}(r) - \boldsymbol{p}(r+1))\|_\infty = \|\boldsymbol{p}(r)(\mathbf{I} - \boldsymbol{\Pi}(r))\|_\infty \leqslant \frac{1}{r} \tag{16}$$

where $\|\cdot\|_\infty$ is the max norm of the finite-dimensional vector $\cdot$.

To calculate the stopping point r_{stop}, a tolerance of $\eta (0 < \eta \leqslant 1)$ is specified for the relative error such that

$$\frac{\|(\boldsymbol{p}(r) - \boldsymbol{p}(r+1))\|_\infty}{\|(\boldsymbol{p}(r))\|_\infty} \leqslant \eta \quad \forall r \geqslant r_{\text{stop}} \tag{17}$$

The objective is to obtain the least conservative estimate for r_{stop} such that the dominant elements of the probability vector have smaller relative errors than the remaining elements. Since the minimum possible value of $\|(\boldsymbol{p}(r))\|_\infty$ for all r is $1/n$, where n is the dimension of $\boldsymbol{p}(r)$, the best worst-case value of the stopping point is obtained from equations (16) and (17) as

$$r_{\text{stop}} \equiv \text{int}\left(\frac{n}{\eta}\right) \tag{18}$$

where $\text{int}(\cdot)$ is the integer part of the real number $\cdot$.

3.5 Anomaly evolution and pattern identification

Behavioural pattern changes may take place in dynamic systems owing to accumulation of faults and progression of anomalies. The pattern changes are quantified as deviations from the nominal pattern (i.e. the probability distribution at the nominal condition). The resulting anomalies (i.e. deviations of the evolving patterns from the nominal pattern) are characterized by a scalar-valued function, called the *anomaly measure* ψ. The anomaly measures at slow time epochs $\{t_1, t_2, \ldots\}$ are obtained as

$$\psi^k \equiv d(\boldsymbol{p}^k, \boldsymbol{p}^0)$$

where $d(\cdot, \cdot)$ is an appropriately defined distance function. In this case, the distance function has been chosen to be the norm of the difference between

the probability vector at slow time epoch t_0 and the probability vector at the nominal condition so that a possible choice for anomaly measure is

$$\psi^k \equiv \|\boldsymbol{p}^k - \boldsymbol{p}^0\|_2 \tag{19}$$

where $\|\cdot\|_2$ is the Euclidean norm of $\cdot$.

The major advantages of STSA for anomaly detection are as follows:

(a) robustness to measurement noise and spurious signals [**17**];
(b) adaptability to low-resolution sensing due to coarse graining in space partitions [**13**];
(c) capability for early detection of anomalies because of the sensitivity to signal distortion and real-time execution on commercially available inexpensive platforms [**14**, **15**].

3.6 Summary of STSA anomaly detection

The STSA procedure of anomaly detection is summarized as follows:

(a) acquisition of time series data from appropriate response variable(s) under the nominal condition at slow time epoch t_0, when the system is assumed to be in the healthy state (i.e. zero anomaly measure);
(b) generation of the wavelet transform coefficients, obtained with an appropriate choice of the wavelet basis [**17**, **22**];
(c) maximum entropy partitioning of the wavelet space at the nominal condition (see section 3.2), and generation of the corresponding symbol sequence (note that the partitioning is fixed for subsequent time epochs);
(d) construction of the D-Markov machine states from the symbol alphabet size $|\Sigma|$ and the window length D, and generation of the state probability vector $\boldsymbol{p}^0$ at time epoch t_0;
(e) time series data acquisition at subsequent slow time epochs, $t_1, t_2, \ldots, t_k, \ldots$, and their conversion to the wavelet domain to generate respective symbolic sequences based on the partitioning at time epoch t_0;
(f) generation of the state probability vectors $\boldsymbol{p}^1, \boldsymbol{p}^2, \ldots, \boldsymbol{p}^k, \ldots$ at slow time epochs, $t_1, t_2, \ldots, t_k, \ldots$ from the respective symbolic sequences using the finite state machine constructed at time epoch t_0;
(g) computation of scalar anomaly measures $\psi^1, \psi^2, \ldots, \psi^k, \ldots$ at time epochs $t_1, t_2, \ldots, t_k, \ldots$.

4 RESULTS OF STSA-BASED ANOMALY DETECTION

This section presents the results of anomaly detection based on simulated time series data of pressure oscillations in the pulse combustor model at different values of the tailpipe friction coefficient f, which is assumed to be quasi-stationary on the fast timescale but gradually changing on the slow timescale. The desired goal of the pulse combustor model is to attain constant-amplitude self-sustained oscillations, which is considered as the nominal behaviour [**5**].

4.1 Simulation runs and STSA analysis

The governing equations of the pulse combustor model are solved as a system of coupled non-linear ordinary differential equations (see section 2). Simulation runs are conducted to generate time series data of pressure oscillations during the period $1.0\ \text{s} \leqslant t \leqslant 1.2\ \text{s}$ after the initial transients have died out such that the results are not sensitive to the choice of the initial conditions. The combustor pressure exhibits self-sustained oscillations at $f \approx 0.0300$, which is considered as the desired nominal behaviour.

The friction coefficient is monotonically decreased by $\Delta f = 0.0005$ from the nominal value of $f = 0.0300$ to represent a gradual reduction in the drag force at consecutive slow time epochs. Thus, the time series data profiles of pressure oscillations are obtained from a family of simulation runs at different values of f ranging from 0.0300 down to 0.0235. Each member of this family of time series data is analysed using the STSA-based anomaly detection procedure as described in section 3 (in particular, see section 3.6) to generate the corresponding state probability vectors. Anomaly measures are then calculated following equation (19).

As stated earlier in section 3.3, the alphabet size for partitioning and the window depth are chosen to be $|\Sigma| = 8$ and $D = 1$ respectively (see sections 3.2 and 3.3). Further increase in the alphabet size $|\Sigma|$ and depth D creates a larger number of states, many of them having very small or zero probabilities with no significant gain in performance.

The STSA algorithm allows detection of a small reduction in f and is computationally very fast in the sense that the code execution time is insignificant relative to the time interval between consecutive slow time epochs. The wavelet basis for partitioning is chosen to be gaus2 [**27**] (see section 3.2) which provides better results than the wavelet bases of the Daubechies family [**21**] because the gaus2

wavelet base closely matches the shape of the pressure oscillations [**17**]. The length of each symbol sequence used in this paper is 20 000, which satisfies the stopping rule in equation (18) for tolerance $\eta = 4 \times 10^{-4}$ and the number n of states equal to 8.

4.2 Effect of friction coefficient on combustor dynamics

As seen in the upper left-hand plot of Fig. 5, the combustor pressure exhibits self-sustained oscillations at $f \approx 0.0300$. Since these oscillations yield higher rates of heat transfer and lower pollutant emission than steady combustion, $f = 0.0300$ is considered to be a design parameter for the nominal operating condition. As f gradually decreases owing to changes in the drag force and due to wear, fatigue and corrosion in the mechanical structures of the tailpipe, fluctuations in the pressure oscillation amplitude start to evolve. This phenomenon is seen in the first and third rows of plots in Fig. 5. The flame is seen to be extinguished abruptly at $f \approx 0.0255$, as seen in

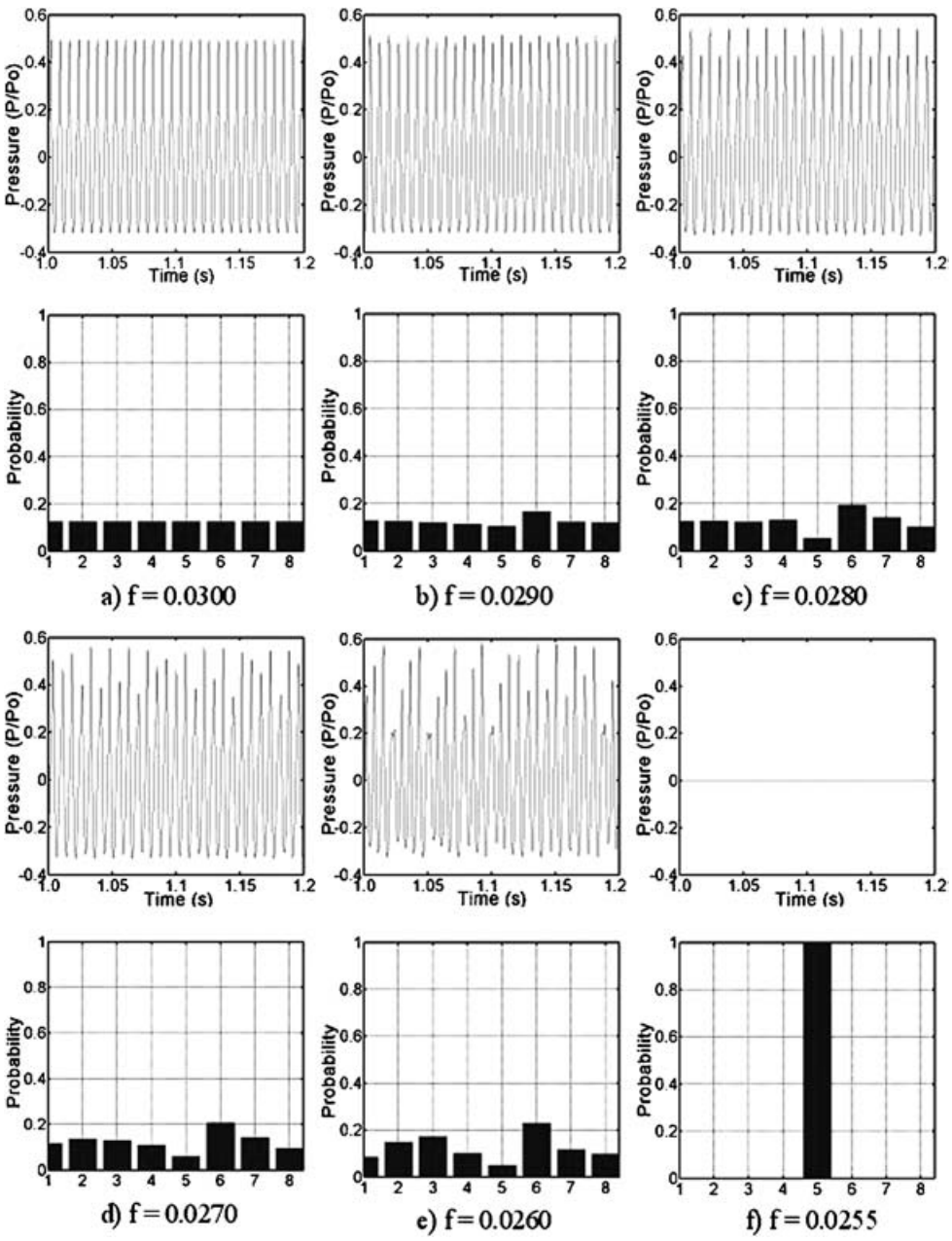

Fig. 5 Profiles of pressure oscillations and corresponding histograms of state probability distribution

the upper plot of the pair in Fig. 5(f). The rationale for these effects on the combustor dynamics due to changes in friction coefficient f is briefly explained below [**1**].

It is evident from equation (5) that the role of the friction coefficient f is to retard the gas flow in the tailpipe in both the forward and the reverse directions. For a high friction coefficient (e.g. $f > 0.035$), the gas flow is significantly slowed, which essentially damps out the oscillations. This phenomenon reduces the temperature and hence the amplitude of pressure oscillations, ultimately leading to steady combustion [**1**]. As the friction coefficient decreases to $f = 0.030$, sustained oscillations at nearly constant amplitude are observed. The state of constant-amplitude pressure oscillations, which is the desired mode of operation in pulse combustors, is identified as the nominal condition. Upon reduction in the friction coefficient below the nominal value, i.e. $f < 0.030$, the efflux of hot gases from the combustion chamber increases. This phenomenon leads to inadequate mixing of hot gases with fresh reactants and lowers the combustor temperature. Reduction in the tailpipe friction coefficient implies lower retardation and hence delayed flow reversal. Thus, at sufficiently low values of friction coefficient, the returning gases do not enter the combustion chamber soon enough to reignite the fresh charge. Upon further reduction in the friction coefficient below the critical value, i.e. $f < 0.0255$, the flame is extinguished with initial transient period of intermittent combustion, which is characterized by extinction and re-ignition events.

4.3 Discussion of pertinent results

The six pairs of plots in Fig. 5 show steady state time series data for the time range $1.0\ \text{s} \leqslant t \leqslant 1.2\ \text{s}$ of the combustor pressure response and the corresponding histograms of state probability distribution at six different values of the tailpipe friction coefficient, $f = 0.0300$, 0.0290, 0.0280, 0.0270, 0.0260, and 0.0255, exhibiting gradual reduction. In each pair of plots Figs 5(a) to (f), the upper plot exhibits the zero mean steady state time series data of pressure response. Histograms in the corresponding lower plots show the evolution of the state probability vector resulting from monotonic reduction in f. This observation signifies how the patterns, represented by probability distribution histograms, gradually change from a uniform distribution (i.e. maximum entropy) to a delta distribution (i.e. minimum entropy).

The upper plot of the pair in Fig. 5(a) shows the pressure response at the nominal condition ($f = 0.0300$) when the anomaly measure is taken to be zero, which is considered as the reference point. As seen in the plot, the combustor model yields (nearly) constant-amplitude pressure oscillations. The uniform distribution is seen from the histogram at the lower plot of the pair in Fig. 5(a), which has the largest entropy [**23**], implying that the least amount of statistical information on anomalies and incipient faults can be extracted from the corresponding time series data.

The pressure responses in the upper plots of the pairs in both Fig. 5(b) and Fig. 5(c) obtained at $f = 0.0290$ and $f = 0.0280$ respectively show alternate pulses with lower peak amplitudes. This phenomenon is one of the possible routes to chaos [**28**]. Such effects in thermal pulse combustors have also been reported by Daw *et al.* [**3**] and In *et al.* [**10**]. The corresponding lower plots exhibit deviations from the uniform probability distribution (see the lower plot of the pair in Fig. 5(a)). This is evidence that small changes in the values of friction coefficient are reflected in the patterns of probability distribution histograms. As f decreases, the changes in the statistics of time series data are captured in the new patterns of histograms that have diminishing entropy, implying more information on anomalies or incipient faults.

The pressure oscillations in the upper plots in the pairs in Figs 5(d) and (e) obtained at $f = 0.0270$ and $f = 0.0260$ respectively exhibit the appearance of oscillations of varying amplitudes and the combustion process tends to become irregular. The histograms of probability distributions in the corresponding lower plots shows further deviation from the uniform distribution at $f = 0.0300$.

The upper plot in the pair in Fig. 5(f) exhibits the steady state pressure response at $f = 0.0255$. At this point, initial intermittent combustion, which is characterized by extinction and re-ignition events, takes place. Thereafter, the flame is extinguished owing to the rapid drop in combustor temperature. The plot, however, shows only the steady state response, which indicates flame extinction with no pressure oscillations. The corresponding lower plot shows the delta distribution (i.e. zero entropy), indicating complete loss of pressure oscillations as all data fall into a single state that includes zero. At this point, complete information on the anomaly pattern is available.

The wavelet space data at the nominal condition $f = 0.0300$ were partitioned using the maximum-entropy principle, which led to uniform probability distribution (i.e. maximum entropy) among the states as shown in the lower plot of the pair in Fig. 5(a).

In contrast, for $f = 0.0255$, the entire probability distribution is concentrated in only one state as seen in the lower plot of the pair in Fig. 5(f), which indicates complete attenuation of the pressure signal due to flame extinction. Therefore, as the tailpipe friction coefficient decreases, the uniform distribution (i.e. maximum entropy) under nominal condition degenerates towards the delta distribution (i.e. zero entropy) for flame extinction. In the intermediate stages, gradual degradation can be quantitatively evaluated using the information from the state probability vectors. The sharp change in pressure response between $f = 0.0260$ and $f = 0.0255$ is possibly due to a bifurcation in the combustion dynamics, which is also analogous to a phase transition in the thermodynamic sense [**18**, **29**].

Figure 6 exhibits the profile of normalized anomaly measures obtained by STSA of pressure oscillations. The region towards the right of $f = 0.0255$ in Fig. 6 is the flame extinction region with no pressure oscillations and the region towards the left consists of self-oscillation modes. In the self-oscillation region, small changes in the anomaly parameter f can be detected, as seen in the increasing deviation in the anomaly measure from the nominal value at which anomaly measure is zero. It is observed from the anomaly profile that the slope of the anomaly measure sharply changes between $f = 0.0260$ and $f = 0.0255$, indicating a transition from self-oscillations to flame extinction. Once the flame is extinguished, the anomaly measure profile becomes flat with indication of no further change. It is emphasized that the anomaly measure is relative to the nominal condition which is chosen *a priori* and should not be construed as the actual damage at an absolute level.

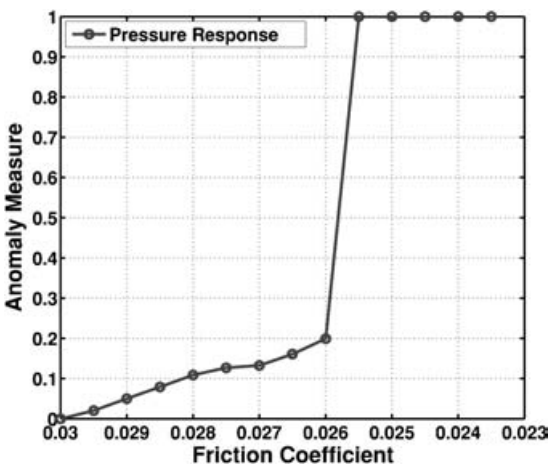

Fig. 6 Anomaly measure for decreasing tailpipe friction coefficient

5 SUMMARY AND CONCLUSIONS

Early detection of gradually evolving anomalies (i.e. deviations from the nominal behaviour) is essential for enhancement of structural integrity, operation reliability, and performance monitoring in thermal pulse combustors. This paper presents the STSA of observable process variables for detection of precursors leading to combustion instability and eventual flame extinction. Time series data of pressure fluctuations, generated from a non-linear dynamic model of a thermal pulse combustor [**1**], are analysed using STSA for detection of statistical pattern changes relative to the nominal condition occurring in the data due to changes in the tailpipe friction coefficient.

The algorithm of STSA-based anomaly detection is built upon the principles of *information theory* and *symbolic dynamics*. A comparison of the STSA approach with other pattern recognition techniques, such as PCA and ANNs, has been recently reported in the literature for electronic circuits [**14**] and mechanical systems [**15**], where the superior performance of STSA was demonstrated in terms of early detection of anomalies in real time.

Preliminary evaluation of the method has been conducted by simulation experiments on a lumped-parameter model of a generic thermal pulse combustor for early detection of combustion instability. The adopted model has been widely used with small modifications for simulation of the non-linear dynamics in thermal pulse combustors [**1–5**, **11**]. The simulation results show that gradual reduction in the tailpipe friction coefficient can be identified from the derived patterns sufficiently in advance of flame extinction. Since the transition to unstable combustion dynamics due to variations in different parameters are found to follow similar routes, the conclusions of the paper can also be useful for detecting other types of anomalies in experimental combustors.

Further theoretical, computational, and experimental research is necessary before the STSA-based anomaly detection tool can be considered for incorporation into the instrumentation and control system of commercial-scale pulse combustors. Specifically, the lumped-parameter model needs to be augmented by a computational fluid dynamics model of a thermal pulse combustor before experimental validation of the STSA-based anomaly detection on a laboratory-scale apparatus. The STSA method for anomaly detection is a pattern identification tool that is independent of the signal type and source.

ACKNOWLEDGEMENTS

This work has been supported in part by the US Army Research Laboratory and the US Army Research Office under Grant DAAD19-01-1-0646.

REFERENCES

1 **Richards, G. A., Morris, G., Shaw, D., Kelley, S.,** and **Welter, M.** Thermal pulse combustion. *Combust. Sci. Technol.*, 1993, **94**, 57–85.
2 **Fichera, A., Loseno, C.,** and **Pagano, A.** Experimental analysis of thermo combustion instability. *Appl. Energy*, 2001, **69**, 101–117.
3 **Daw, C. S., Thomas, J. F., Richards, G. A.,** and **Narayanaswamy, L. L.** Chaos in thermal pulse combustion. *Chaos*, 1995, **5**, 662–670.
4 **Edwards, K. D., Finney, C. E. A., Nguyen, K.,** and **Daw, C. S.** Application of nonlinear feedback control to enhance the performance of a pulsed combustor. In Proceedings of the 2000 Spring Technical Meeting of the Central States Section of the Combustion Institute, Indianapolis, Indiana, USA, 2000, pp. 249–254.
5 **Rhode, M., Rollins, R., Markworth, A., Edwards, K., Nguyen, K., Daw, C.,** and **Thomas, J.** Controlling chaos in a model of thermal pulse combustion. *J. Appl. Physics*, 1995, **78**, 2224–2232.
6 **Abarbanel, H.** *The analysis of observed chaotic data*, 1996 (Springer-Verlag, New York).
7 **Kantz, H.** and **Schreiber, T.** *Nonlinear time series analysis*, 1996 (2nd edition, 2004 Cambridge University Press, Cambridge).
8 **Edwards, K. D., Nguyen, K.,** and **Daw, C. S.** Enhancing the operation of a pulsed combustor with trajectory correction control. In Proceedings of the Second Joint Meeting of the U.S. Sections of the Combustion Institute, Oakland, California, USA, 2002, 107.
9 **Khatkhate, A., Gupta, S., Ray, A.,** and **Keller, E.** Life extending control of mechanical systems using symbolic time series analysis. In Proceedings of the American Control Conference, Minnesota, USA, 2006, pp. 3765–3770.
10 **In, V., Spano, M., Neff, J., Ditto, W., Daw, C., Edwards, K.,** and **Nguyen, K.** Maintenance of chaos in a computational model of thermal pulse combustor. *Chaos*, 1997, **7**, 605–613.
11 **Datta, S., Mukhopadhyay, A.,** and **Sanyal, D.** Modeling and analysis of the nonlinear dynamics of a thermal pulse combustor. In Proceedings of the 42nd AIAA–ASME–SAE–ASEE Joint Propulsion Conference, Sacramento, California, USA, July 2006, paper AIAA-2006-4396.
12 **Crutchfield, J. P.** and **Young, K.** Inferring statistical complexity. *Phys. Rev. Lett.*, 1989, **63**, 105–108.
13 **Ray, A.** Symbolic dynamic analysis of complex systems for anomaly detection. *Signal Processing*, 2004, **84**(7), 1115–1130.
14 **Chin, S., Ray, A.,** and **Rajagopalan, V.** Symbolic time series analysis for anomaly detection: a comparative evaluation. *Signal Processing*, (September 2005), **85**(9), 1859–1868.
15 **Gupta, S., Ray, A.,** and **Keller, E.** Symbolic time series analysis of ultrasonic data for early detection of fatigue damage. *Mech. Systems Signal Processing*, 2006 (in press), available online at www.ScienceDirect.com
16 **Daw, C., Finney, C.,** and **Tracy, E.** A review of symbolic analysis of experimental data. *Rev. Scient. Instrum.*, 2003, **74**(2), 915–930.
17 **Rajagopalan, V.** and **Ray, A.** Symbolic time series analysis via wavelet-based partitioning. *Signal Processing* (in press), available online at www.ScienceDirect.com
18 **Beck, C.** and **Schlögl, F.** *Thermodynamics of chaotic systems: an introduction*, 1993 (Cambridge University Press, Cambridge).
19 **Davidchack, R., Lai, Y., Bolt, E.,** and **Dhamala, H.** Estimating generating partitions of chaotic systems by unstable periodic orbits. *Phys. Rev. E*, 2000, **61**, 1353–1356.
20 **Kennel, M.** and **Buhl, M.** Estimating good discrete partitions form observed data: symbolic false nearest neighbors. *Phys. Rev. E*, 2003, **91**(8), 84–102.
21 **Mallat, S.** *A wavelet tour of signal processing*, 2nd edition, 1998 (Academic Press, New York).
22 **Rajagopalan, V.** and **Ray, A.** Wavelet-based space partitioning for symbolic time series analysis. In Proceedings of 44th IEEE Conference on *Decision and control* and European Control Conference, Seville, Spain, December 2005, pp. 5245–5250 (IEEE New York).
23 **Cover, T. M.** and **Thomas, J. A.** *Elements of information theory*, 1991 (John Wiley, New York).
24 **Lind, D.** and **Marcus, M.** *An introduction to symbolic dynamics and coding*, 1995 (Cambridge University Press, Cambridge).
25 **Bapat, R.** and **Raghavan, T.** *Nonnegative matrices and applications*, 1997 (Cambridge University Press, Cambridge).
26 **Ray, A.** Signed real measure of regular languages for discrete event supervisory control. *Int. J. Control*, 2005, **78**(12), 949–967.
27 *MATLAB Wavelet Toolbox*, 2006 (Mathworks Inc., Natick, Massachusetts).
28 **Hilborn, R. C.** *Chaos and nonlinear dynamics*, 2nd edition, 2000 (Oxford University Press, Oxford).
29 **Goldenfeld, N.** *Lectures on phase transitions and the renormalization group*, 1992 (Perseus Books, Reading, Massachusetts).

APPENDIX

Notation

A_e tailpipe cross-sectional area (m^2)
A_s combustor surface area (m^2)

B	pre-exponential factor for single-step chemical kinetics ($m^3/kg\,K^{1/2}\,s^1$)
C_p	specific heat at constant pressure (J/kg K)
D	window length on a symbolic sequence
D_{tp}	diameter of the tailpipe (m)
f	friction coefficient (dimensionless)
h	convective heat transfer coefficient ($W/m^2\,K$)
L_{c1}	first characteristic length $= V/A_s$ (m)
L_{c2}	second characteristic length $= V/A_e$ (m)
L_{tp}	length of the tailpipe (m)
m	size of the alphabet set $= \lvert\Sigma\rvert$
$\dot{m}_e$	mass flowrate at combustor exit (kg/s)
$\dot{m}_i$	mass flowrate at combustor inlet (kg/s)
$\boldsymbol{p}^k$	state probability vector at time epoch t_k
P	pressure in the combustion zone (Pa)
$P(\cdot)$	probability of the event $\cdot$
$\tilde{P}$	normalized pressure $= P/P_0$ (dimensionless)
P_e	pressure at the tailpipe entrance (Pa)
$\tilde{P}_e$	normalized tailpipe pressure $= P_e/P_0$ (dimensionless)
P_0	ambient pressure (Pa)
q_j	jth state of the finite state machine
Q	set of all states of the finite state machine
R	gas constant $= (\gamma - 1)C_p/\gamma$ (J/kg K)
$\dot{R}_f$	fuel reaction rate ($kg/m^3\,s$)
S	dynamic systems entropy of the symbol sequence
t	continuous time (s)
t_k	slow time epoch
T	temperature in the combustion zone (K)
$\tilde{T}$	normalized temperature $= T/T_0$ (dimensionless)
T_a	activation temperature (K)
T_e	temperature at the tailpipe entrance (K)
T_w	wall temperature in the combustion zone (K)
$\tilde{T}_e$	normalized tailpipe temperature $= T_e/T_0$ (dimensionless)
$\tilde{T}_w$	normalized wall temperature $= T_w/T_0$ (dimensionless)
T_0	ambient temperature (K)
u	gas velocity in the tailpipe (m/s)
$\tilde{u}$	$= u/(L_{c2}/\tau_f)$ (dimensionless)
V	volume of the combustor (m^3)
Y_f	average fuel mass fraction in the combustor chamber (dimensionless)
Y_{fi}	fuel mass fraction at the combustor inlet (dimensionless)
Z_e	$= \dot{m}_e/V$ ($kg/m^3\,s$)
Z_i	$= \dot{m}_i/V$ ($kg/m^3\,s$)
γ	ratio of specific heats (dimensionless)
Δh_c	enthalpy of combustion (J/kg)
ν_0	stoichiometric oxygen-fuel ratio by mass (dimensionless)
$\boldsymbol{\Pi}^k$	state transition matrix at time epoch t_k
ρ	density in the combustion zone (kg/m^3)
ρ_0	ambient density (kg/m^3)
σ	symbol in a symbolic sequence
Σ	alphabet set
τ_c	characteristic chemical reaction time (s)
τ_f	characteristic flow time (s)
τ_h	characteristic heat transfer time (s)
ψ^k	anomaly measure computed at time epoch t_k
Ω	phase space of a dynamic system